Available online at www.sciencedirect.com
ScienceDirect
Surface Science 601 (2007) 5142–5147
SURFACE SCIENCE
www.elsevier.com/locate/susc

Growth and characteristics of lead sulfide nanocrystals produced by the porous alumina membrane

Jung-Hsuan Chen *, Chuen-Guang Chao, Jong-Chyan Ou, Tzeng-Feng Liu

Department of Materials Science and Engineering, National Chiao Tung University, Hsinchu 300, Taiwan, ROC

Available online 29 April 2007

Abstract

Lead sulfide (PbS) nanocrystals were formed by using Pb nanowires reacted with hydrogen sulfide (H_2S) gas. The structure and composition of the as-prepared nanocrystals were confirmed by scanning electron microscopy, X-ray diffraction, transmission electron microscope and energy dispersive X-ray spectroscopy. According to the differential scanning calorimeter analysis, the PbS nanocrystals in a cubic structure owned excellent thermal stability. Furthermore, the optical properties including photoluminescence (PL) and Raman scatting spectrum were also measured. The PL emission measurement of the PbS nanocrystal showed that there was an orange–red emission peak located around 655 nm. A significant quantum confinement effect made the energy gap of PbS produce a blue shift from 0.41 eV to 1.9 eV.

Keywords: PbS; Nanocrystal; Sulfization; Thermal stability; Quantum confinement

1. Introduction

In recent years, there has been a dramatic proliferation of research concerned with low dimensional materials. The physical properties of one dimensional and quasi-one-dimensional structure have drawn much attraction for fundamental studies and for practical application in electronics, optoelectronics and thermoelectronics, etc. Nanomaterials in the templates exhibit both optical and transport anisotropy. The effect of the template in structurally defined nanomaterials is the dielectric enhancement of the optical anisotropic due to the layered structure of the ensemble. An appropriate infill, such as II–VI or IV–VI semiconductors, could produce the significant broadness of the electronic transitions resulting from the quantum confinement effect. Because of the distinguished optical and electronic properties, the control of the size and morphology of nanomaterials has been a primary topic [1].

Lead sulfide (PbS) is a narrow band gap semiconductor material that can be readily prepared as nanostructure exhibiting strong quantum confinement effect of both charge carriers [2]. As the ratio of the surface to volume is large in the case of nanostructure materials, it is possible to observe some distinctive properties of relative bulk materials.

PbS nanostructures have been fabricated in polymers hosts [3,4], mesoporous silica templates [5] and glass hosts [6] with different morphologies such as hollow sphere [7], rectangular, cubic [8], star-like [9] or clover-like structures [10]. PbS nanostructures are potentially useful in solar cell [11,12], optical switches [13] and light emitting diodes. For the manufactures of electric or optical devices, some properties of PbS have to be concerned seriously, thermal stability, mechanical strength ...... for instance. As technology requirements increase, so does demand for precisely controlled and predictive nanostructure growth. The purpose of the present work was to investigate the relationship between the nanostructure and theirs physical properties, such as, thermal characterization and optical properties, etc. The study we present in the present paper is an attempt

* Corresponding author. Tel.: +886 3 5731809; fax: +886 3 5724727.
E-mail address: cgchao@faculty.nctu.edu.tw (J.-H. Chen).

0039-6028/$ - see front matter © 2007 Elsevier B.V. All rights reserved.
doi:10.1016/j.susc.2007.04.228

to supplement the findings of these earlier studies. It differs from previous studies, however, in the way a novel process to fabricate PbS nanocrystals in the porous alumina membrane is offered. PbS nanocrystals were formed by using Pb nanowires reacted with hydrogen sulfide (H_2S) gas. The PbS nanocrystals produced in this process could be dispersed well in the alumina membrane. When the nanocrystals aggregate together, the quantum effect would decrease or disappear. Furthermore, this process is more suitable to produce the large area PbS nanocrystals without aggregation. Due to the heating and pressure process, the substrate must be chemically stable and able to maintain its porous structure. Therefore, the porous alumina membrane is a typical material used as the template.

2. Experimental details

A porous alumina membrane used as a template was produced after the anodization of an aluminum foil in the acid solution [14]. The polished Al foil (99.7%) was anodized using platinum plate as the counter electrode in a 10% sulfuric acid solution (H_2SO_4, 98%) at 281 K for 1 h and an applied voltage 18 V. The nanochannel structures with diameter of 20 nm were obtained on the Al substrate.

PbS nanocrystals were fabricated by pressure injection and sulfization process in the porous alumina membrane. A piece of Pb metal and an anodic aluminum oxide template were placed inside an ultra-vacuum chamber. After the chamber was heated to 673 K, a hydraulic force was applied to inject the Pb melt into the nanopores as described in the previous study [15–17]. We adopted a quenching procedure during Pb melt solidification to separate the nanowire and the remaining metal on the anodic alumina template. This procedure could provide a steep temperature gradient between the nanowires and remaining metal. We could easily obtain the lead nanowire arrays inside the alumina membrane.

The force F required to overcome the surface tension of melt to fill the pores is estimated by the equation [16]: $P = \frac{F}{A} = \frac{-2\gamma\cos\theta}{r}$. As indicated in this equation, the force is inversely proportional to the radius of the nanochannel (r). That is, getting smaller nanowires needs to apply larger hydraulic force. In our experiment, the specimen area (A) is 1 cm^2, the radius of nanopores is 10 nm, the surface tension (γ) of the Pb melt is 468 dyn/cm and the contact angle (θ) between the melt and the pores is about 106° [18]. Therefore, the critical force of forming the Pb nanowires with a diameter of 20 nm is counted as 2580 N. In order to increase the filling ratio of lead nanowires, using a larger force is essential.

Then, the nanowire arrays were put into a gaseous furnace injected H_2S gas with a flow rate was 30 mL/min and applied a heat treatment at 573 K for 6 h. The PbS nanocrystals were fabricated. Their morphologies were observed by scanning electron microscopy (SEM, JEOL JSM-6500). The compositions and crystallization of nanocrystals were detected by energy dispersive X-ray spectroscopy (EDS, EDAX) and X-ray diffraction (XRD, Siemens D5000). The investigation of the nanostructure was carried out with a Philip Tecnai 20 transmission electron microscope (TEM) operating at 200 kV. The advanced TEM specimen preparation method of using a focused ion beam (FIB) miller applied to prepare the cross-sectional TEM specimen. Coatings of gold were first deposited on to the selected sample area to protect the sample during processing. Using a PerkinElmer Diamond differential scanning calorimeter (DSC), the thermal character was measured. DSC is a thermal analysis technique which is used to measure the temperatures and heat flows associated with transitions in materials as a function of time and temperature. The optical properties including photoluminescence (PL) and Raman spectra were examined at the room temperature by a Jobin-Yvon Spex Fluolog-3 spectrophotometer with a xenon lamp as the excitation light source and a Jobin-Yvon LabRAM HR micro-Raman spectrometer.

3. Results and discussion

3.1. Reaction of lead nanowires and hydrogen sulfide gas

Figs. 1a and b are the images of a porous alumina membrane in which pore diameter was 20 nm and Pb nanowire arrays formed as the hydraulic force was applied. After the 20 nm Pb nanowire arrays were fabricated, a sulfization procedure was proceeded to obtain PbS nanoparticles, as shown in Fig. 1c. The reaction of PbS formation is described as following:

$$Pb_{s,l} + H_2S_{(g)} \rightarrow PbS_{(s)} + H_{2(g)}$$

From the thermodynamics aspect, the Gibbs free energy can be written as

$$\Delta G = -76.18 + 0.042T \ [19] \quad \mathrm{kJ/mol}$$

Based on the thermodynamic calculation, it is a spontaneous reaction as the temperature reaches 573 K and the reaction Gibbs free energy G is −52.11 kJ/mol. All of the Pb nanowires would transform into PbS crystals if the reaction time is long enough. If the exposure time to H_2S gas is too long or the reaction temperature is too high, the formed PbS nanocrystals would aggregate easily on the surface of the porous alumina membrane. Therefore, controlling reaction conditions carefully is essential for the fabrication of PbS nanocrystals.

3.2. Characterizations of lead sulfide nanocrystals in the porous alumina membrane

Microstructure characterization was carried out by X-ray diffraction and scanning electron microscopy in order to determine the crystal structure and to study the surface morphology of the as-prepared PbS nanocrystals. The XRD analysis in Fig. 2 shows that the PbS phase appears after the reaction of Pb and H_2S gas occurred. The three

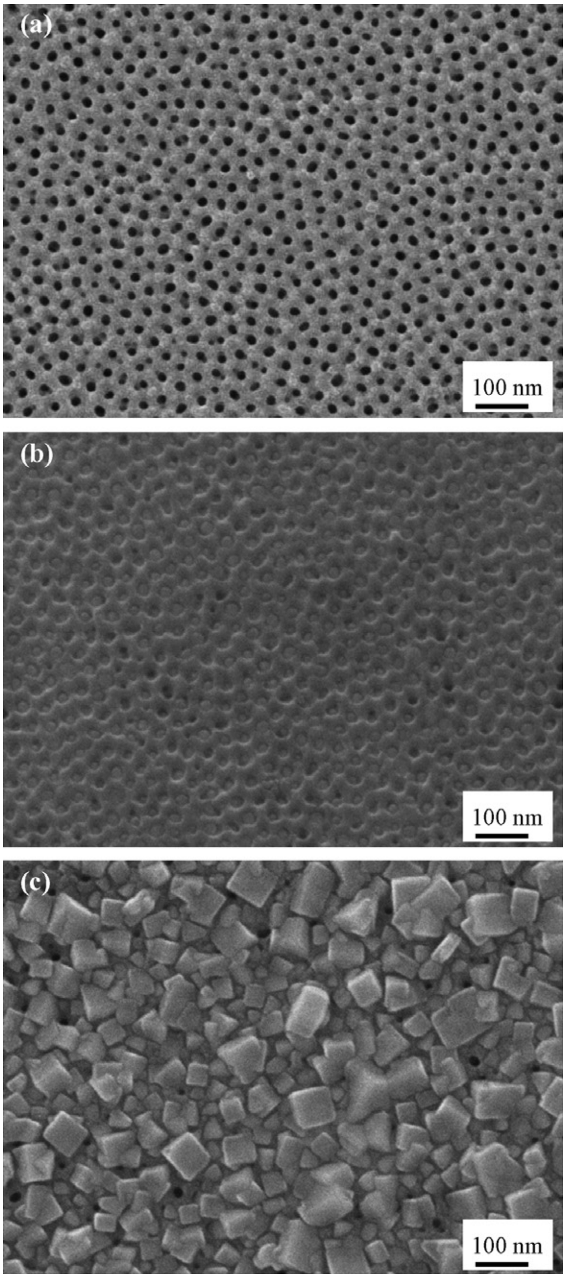

Fig. 1. SEM images (a) a porous alumina membrane with an ordering pore diameter of 20 nm, (b) Pb nanowire arrays fabricated by vacuum pressure injection process and (c) PbS nanoparticles.

peaks of PbS nanocrystals are the same as the (1 1 1), (2 0 0) and (2 2 0) peaks of bulk PbS. The PbS phase is identified to crystallize in cubic crystalline lattice (Fm3m, space group = 225, JCPDS No. 03-0665) with the lattice constant $a = 0.59362$ nm [20]. Atomic coordinates are (0,0,0) and (0,1/2,1/2) for Pb and (1/2,1/2,1/2) and (1,1,1/2) for S. In Fig. 2, the diffraction peaks of non-reacted Pb and substrate of Al coming from the porous alumina template also exist simultaneously.

More structure characteristics of PbS nanocrystals outside the pores of the porous alumina membrane can be obtained from the TEM analysis. The low-magnification

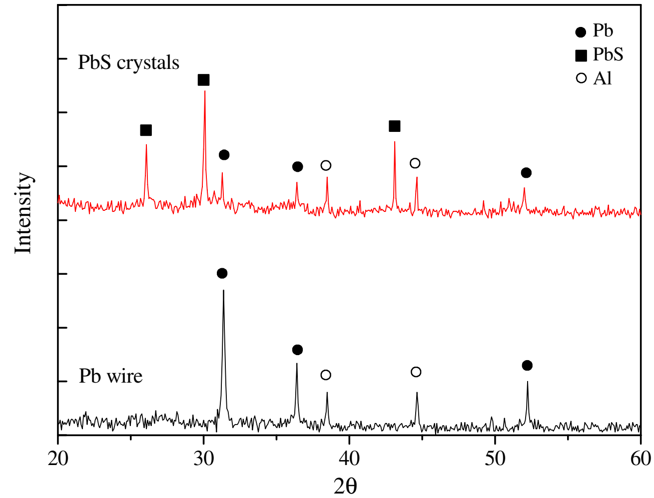

Fig. 2. X-ray diffraction profiles of Pb nanowires and PbS nanocrystals.

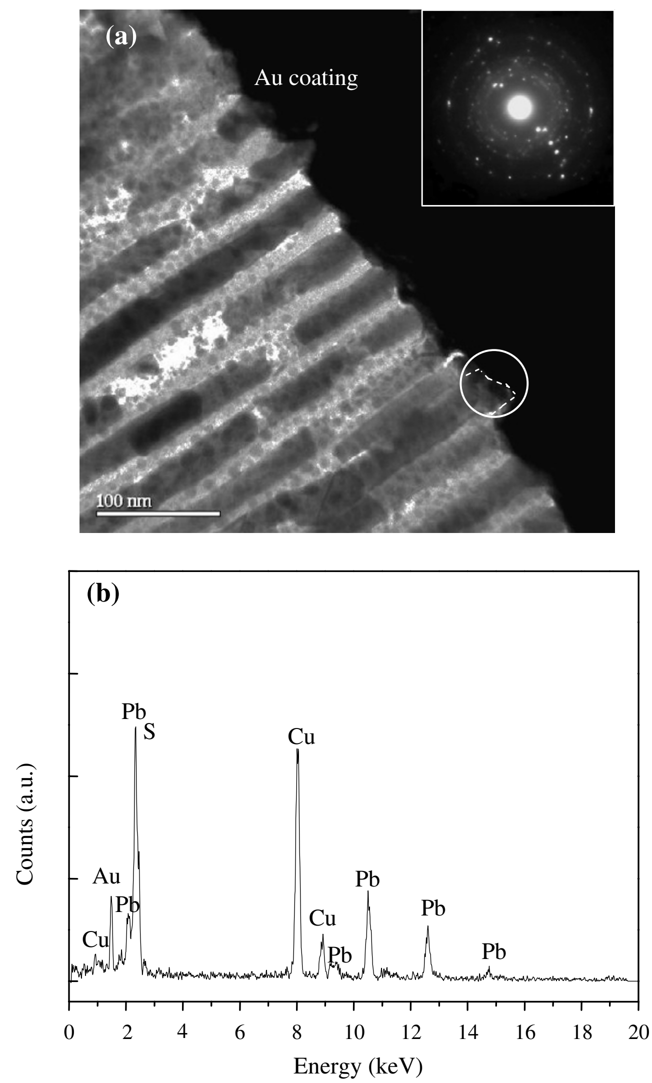

Fig. 3. (a) Low-magnification TEM image and the corresponding selective-area electron diffraction pattern of a PbS nanoparticle (the circular area), and (b) energy-dispersive X-ray spectrum recorded from a PbS nanoparticle (the circular area in (a)).

cross-sectional structures of PbS particle is presented in the bright field TEM image shown in Fig. 3a. A particle growing out of the pore of the alumina membrane was marked by a circle. According to the selective-area electron diffraction pattern (SAED) of this PbS nanoparticle (marked area), it can be known that the particle growing outside the pore was a polycrystal structure and comprised several crystals. The EDS analysis was performed with TEM to show the composition of PbS nanocrystals marked in Fig. 3a. From the EDS spectrum in Fig. 3b, the nanocrystals are judged to consist of Pb and S in the ratio of 1:1 with a statistical error of 5% and exhibit no other signals of elements in the spectrum. The copper and gold signals come from the TEM grid and Au coating. The result corresponds to the results of X-ray diffraction analysis discussed previously. To further confirm this result, high-resolution TEM (HRTEM) images were performed to determine the structure of PbS nanocrystal. The HRTEM images (Fig. 4b–d) of the boxed areas in Fig. 4a further support the nanocrystal nature of PbS. The lattice fringes ($d = 2.97$ Å) observed in those HRTEM images are identical with the distance between the (200) lattice planes.

The DSC curves of the PbS nanocrystals in Fig. 5 shows that there is a variation on the melting point for the Pb samples (bulk and nanowire). The melting temperature decreases from 599.99 K to 596.57 K as its size decreases. For nanocrystals embedded in a matrix, they can melt below the melting point of the bulk materials when the interfaces between embedded nanocrystals and the matrix are incoherent [21]. Therefore, the experiment result agrees well with the theoretical prediction. Furthermore, due to the potential applications in the field of microelectronics and optoelectronics, understanding of the thermal stability of low-dimensional materials is important. Mahmoud and Hamid [22] discussed that an exothermic peak (533.59 K) found in the thermal analysis spectrum attributed to the grain growth for the chemical deposition PbS powders. Moreover, there is a high intensity exothermic peak at 551.72 K in the thermal ingot powders. In our experiment, however, the plot of DSC for PbS nanocrystals provides information that there is no exothermic and endothermic reactions taking place in the sample during temperature range (373–623 K). That means the grain of the PbS nanocrystals grows slightly and non-obviously. This condition

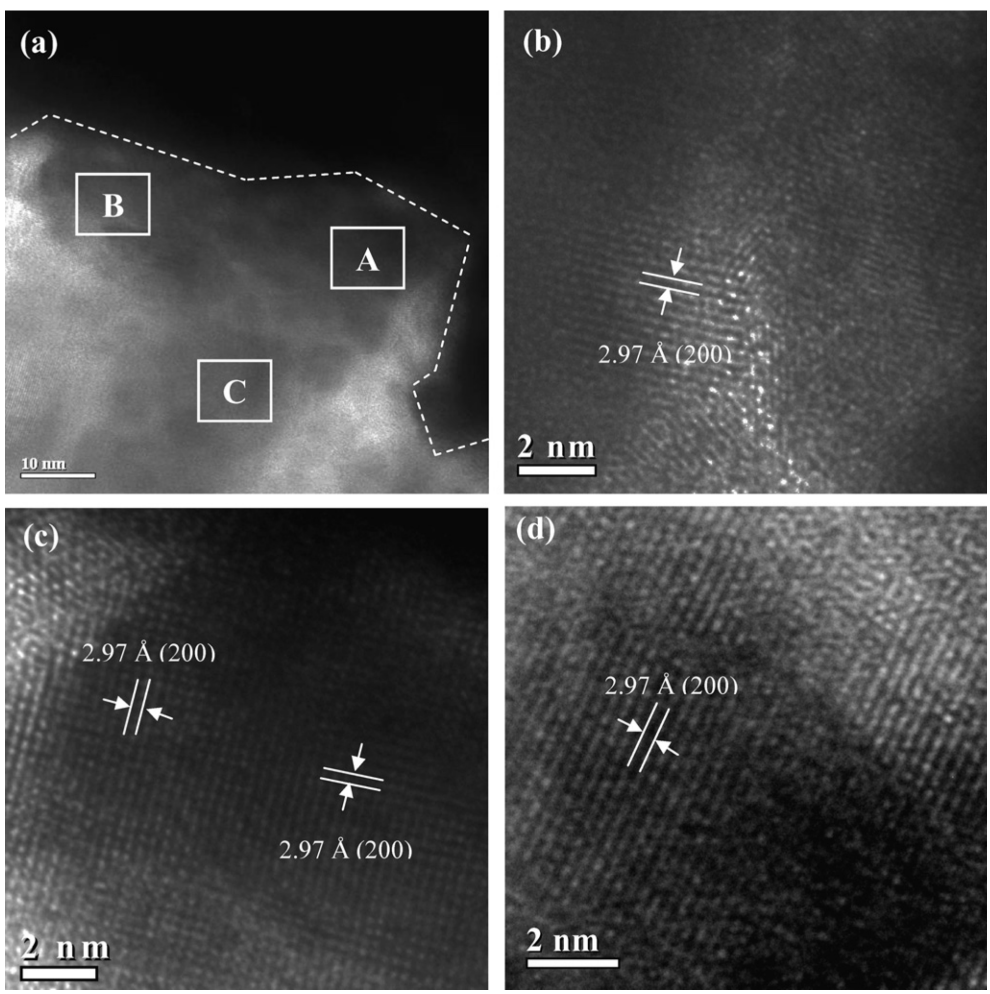

Fig. 4. (a) Enlarged TEM image recorded from the marked area in Fig. 3 (a) High-resolution TEM images of PbS nanocrystals, (b)–(d), recorded from the areas indicated by A, B and C boxes in (a), respectively.

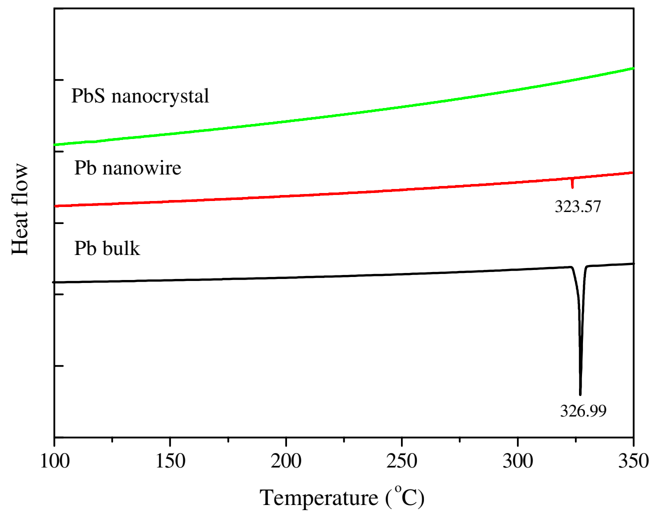

Fig. 5. DSC thermographs of Pb bulk, Pb nanowires and PbS nanocrystals.

might result from the confinement of the nanochannel in the porous alumina membrane. Because the alumina membrane is a ceramic material with the excellent thermal and chemical stability, the interaction between the PbS crystals and substrate does not happen. Therefore, the PbS nanocrystals produced in our process have great thermal stability.

Raman spectroscopy is a fast and nondestructive tool to appreciate crystalline material qualities, including surface conditions and homogeneity, and therefore crystalline samples present sharp Raman peaks while amorphous or polycrystalline samples show very broad Raman peaks. Fig. 6 shows the Raman spectrum of PbS nanocrystals using 632.8 nm excitation wavelength. Four Raman bands from the PbS nanocrystal at 151, 194, 212 and 451 cm^{-1} are observed. Raman shifts usually correspond to the longitudinal optical phonons (LO), the transverse optical phonons

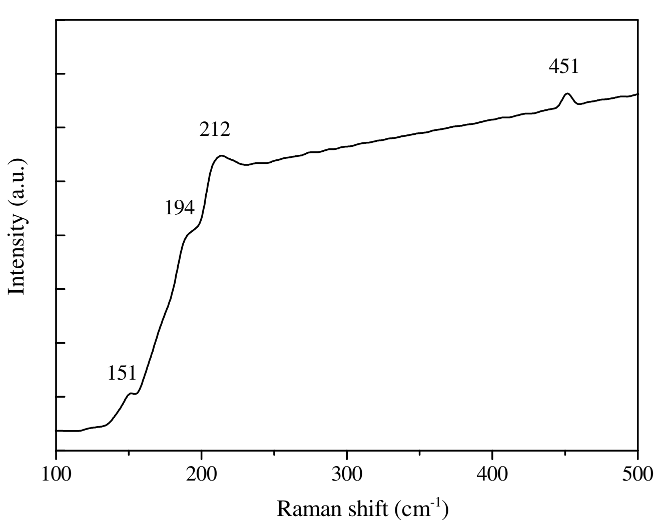

Fig. 6. Raman spectrum of PbS nanocrystals using the He/Ne laser excitation at room temperature.

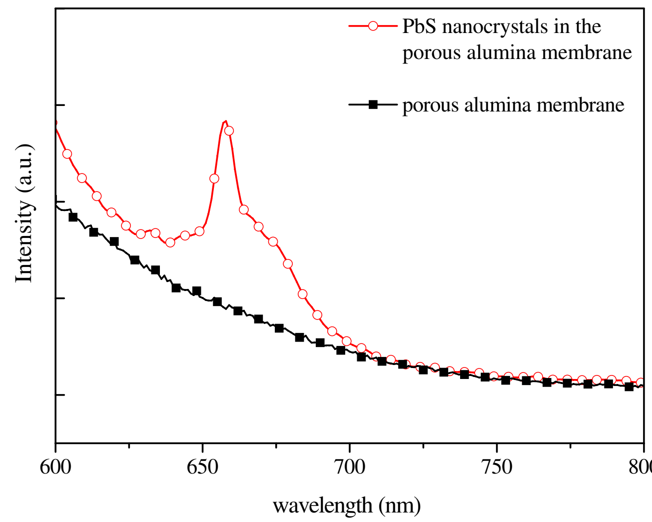

Fig. 7. PL spectrum of PbS nanocrystals. There is an emission peak centered at 655 nm.

(TO) and the surface phonons (SP). The TO and SP modes are difficult to observe in the Raman spectrum due to the symmetry restrictions and low intensities, respectively. As expected, two bands at 212 and 451 cm^{-1} are attributed to the scatterings of the 1LO phonon and 2LO phonon of PbS, respectively [23,24]. A weak band at 151 cm^{-1} assigns to be a combination of transverse acoustic (TA) and TO phonons [25,26]. Furthermore, if the surface to volume ration is large, it will be possible to observe SP mode in the Raman spectrum. In our case, there is a peak at 194 cm^{-1} owing to the SP phonons [24,27].

PbS is an excellent semiconductor material because of its narrow band gap ~0.41 eV and a large exciton Bohr radius of 18 nm [28]. Strong quantum confinement of both charge carriers can be easily achieved by fabricating PbS crystals with a radius less than 18 nm. The photoluminescence emission spectra, shown in Fig. 7, were measured from 600 nm to 800 nm at the room temperature and the excitation wavelength was 514 nm. Fig. 7 indicates that there is no emission signal in the porous alumina membrane but a broad peak located around 655 nm (1.9 eV) appears after PbS nanocrystals produce. The energy transitions in both electron and hole levels of PbS nanocrystals was revealed in four major types, the S_e–S_h, S_e–P_h, P_e–S_h and P_e–P_h transitions [29]. In Fig. 7, the emission peak observed at 1.9 eV corresponds to the S_e–S_h transition which is a lowest energy exciton. The probable explanation about the energy gap of PbS shifts from 0.41 eV to 1.9 eV is indicative of the presence of the quantum confinement effect.

4. Conclusions

In summary, a method to fabricate PbS nanocrystals have been developed. The PbS nanocrystals are synthesized from the reaction of Pb nanowires and H_2S gas. According to the result of X-ray diffraction, PbS nanocrystals are in cubic crystalline structure. The DSC analysis shows that there is no exothermic and endothermic reaction happened in the PbS nanocrystals. That is, the PbS nanocrystals have good thermal stability during temperature range (373–623 K). Four Raman bands, located at 151, 194, 212 and 451 cm^{-1}, from PbS nanocrystals are observed. They are attributed to the scatterings of the combination bands, SP phonon, 1LO phonon and 2LO phonon. The photoluminescence measurement describes the PL behaviors of PbS nanocrystals. A broad emission peaks around 655 nm is observed. Such a large blue shift from 0.41 eV (band gap of the bulk) to 1.9 eV (655 nm) indicates a significant amount of quantum confinement energy. This research may give rise to an alternative method of producing PbS nanostructures and offer future studies more information about PbS nanocrystals.

Acknowledgement

This work was supported by the National Science Council of the Republic of China under the Research Contract No. NSC95-2221 E009-062.

References

[1] Y. Ji, X. Ma, H. Zhang, J. Xu, D. Yang, J. Phys.: Condens. Matter. 15 (2003) 7611.
[2] F.W. Wise, Acc. Chem. Res. 33 (2000) 773.
[3] L. Bakueva, S. Musikhin, M.A. Hines, T.W.F. Chang, M. Tzolov, G.D. Scholes, E.H. Sargent, Appl. Phys. Lett. 82 (2003) 2895.
[4] C. Lü, C. Guan, Y. Liu, Y. Cheng, B. Yang, Chem. Mater. 17 (2005) 2448.
[5] F. Gao, Q. Lu, X. Liu, Y. Yan, D. Zhao, Nanotechnol. Lett. 1 (2001) 743.
[6] G. Tamulaiyis, V. Gulbinas, G. Kodis, A. Dementjev, L. Valkunas, J. Appl. Phys. 88 (2000) 178.
[7] S.F. Wang, F. Gu, M.K. Lu, Langmuir 22 (2006) 398.
[8] Y. Ni, H. Liu, F. Wang, Y. Liang, J. Hong, X. Ma, Z. Xu, Cryst. Growth Des. 4 (2004) 759.
[9] Y. Ma, L. Oi, J. Ma, H. Cheng, Cryst. Growth Des. 4 (2004) 351.
[10] Y. Ni, H. Liu, F. Wang, Y. Liang, J. Hong, X. Ma, Z. Xu, Cryst. Res. Technol. 39 (2004) 200.
[11] R. Plass, S. Pelet, J. Krueger, M. Grätzel, U. Bach, J. Phys. Chem. B 106 (2002) 7578.
[12] J.H. Warner, A.R. Watt, R.D. Tilley, Nanotechnology 16 (2005) 2381.
[13] S.W. Lu, U. Sohling, M. Menning, H. Schmidt, Nanotechnology 13 (2002) 669.
[14] H. Masuda, F. Hasegwa, J. Electrochem. Soc. 144 (1997) L127.
[15] C.C. Chen, C.G. Kuo, C.G. Chao, Jpn. J. Appl. Phys. 44 (2005) 1524.
[16] Z. Zhang, J.Y. Ying, M.S. Dresselhaus, J. Mater. Res. 13 (1998) 1745.
[17] T.E. Huber, M.J. Graf, C.A. Foss Jr., P. Contant, J. Mater. Res. 15 (2000) 1816.
[18] B.B. Alchagirov, A.G. Mozgovoy, Kh.B. Khokonov, High Temp. 41 (2003) 755.
[19] M.W. Chase, C.A. Davies, JANAF Thermochemical Tables, Dow Chemical Company, Thermal Research Laboratory, New York/ American Institute of Physics, 1985.
[20] P. Villars, L.D. Calvert, Pearson's Handbook of Crystallographic Data, The Materials Information Society, 1991.
[21] Z. Zhang, J.C. Li, Q. Jiang, J. Phys. D: Appl. Phys. 33 (2000) 2653.
[22] S. Mahmoud, O. Hamid, FIZIKA A 10 (2001) 21.
[23] T.D. Krauss, F.W. Wise, Phys. Rev. B 55 (1997) 9860.
[24] J.P. Ge, J. Wang, H.X. Zhang, X. Wang, Q. Peng, Y.D. Li, Chem. Eur. J. 11 (2005) 1889.
[25] R. Sherwin, R.J.H. Clark, R. Lauck, M. Cardona, Solid State Commun. 134 (2005) 565.
[26] H. Cao, G. Wang, S. Zhang, X. Zhang, Nanotechnology 17 (2006) 3280.
[27] K.K. Nanda, S.N. Sahu, R.K. Soni, S. Tripathy, Phys. Rev. B 58 (1998) 15405.
[28] M. Fernee, A. Watt, J. Warner, N. Heckenberg, H. Rubinsztein-Dunlop, Nanotechnology 15 (2004) 1328.
[29] J.L. Machol, F.W. Wise, R.C. Patel, D.B. Tanner, Phys. Rev. B 48 (1993) 2819.